Regenerative Therapy 12 (2019) 94–101

Contents lists available at ScienceDirect

Regenerative Therapy

journal homepage: http://www.elsevier.com/locate/reth

Original Article

A distribution-based approach for determining lot sizes in the filling of human-induced pluripotent stem cells

Hirokazu Suigyama [a, *], Masaki Shiokaramatsu [a], Masahiro Kino-oka [b]

[a] Department of Chemical System Engineering, The University of Tokyo, 7-3-1 Hongo, Bunkyo-ku, Tokyo, 113-8656, Japan
[b] Department of Biotechnology, Osaka University, 2-1 Yamadaoka, Suita, Osaka, 565-0871, Japan

ARTICLE INFO

Article history:
Received 31 October 2018
Received in revised form
14 March 2019
Accepted 18 April 2019

Keywords:
Cell manufacturability
Process modeling
Process design
Optimization
Decision-making
Monte Carlo simulation

ABSTRACT

Introduction: Toward the commercial production of human-induced pluripotent stem (hiPS) cells, the process design and operation have to be standardized. Considering the change in cell quality during filling of the hiPS cells into containers, lot sizing during filling also needs to be standardized.
Methods: We present a distribution-based approach that can be used for determining the lot sizes in the filling of hiPS cells by considering change in cell quality during filling. The approach describes the "survival capability" of the cells as a continuous probability distribution, and expresses the change in quality during filling by "trimming" the distribution.
Results: A lognormal distribution was assumed as the survival capability distribution of the cells that were to be filled. The distributions after different filling times were calculated, which were compared with the distribution of the initial filling time regarding the yield of the cells and the similarity. These conditions served as strong quality constraints in determining an economically optimal lot size.
Conclusions: The presented conceptual approach would be effective in determining the lot size considering the change in cell quality during filling. For actual application, measuring the distribution information on the survival capability of hiPS cells is encouraged.

1. Introduction

The demand for human-induced pluripotent stem (hiPS) cells is increasing. In 2014, Kameo et al. [1] presented a characterization of hiPS cell-derived retinal pigment epithelium cell sheets, which were the subject of a clinical study for treating age-related macular degeneration. Sheets of hiPS cell-derived cardiomyocytes, which were developed by Kawamura et al. [2] in 2012, were approved for clinical studies in 2018. A massive and reproducible production of hiPS cell-derived liver buds has been presented by Takebe et al. [3], and these are now being considered for clinical studies. Olmer et al. [4] indicated that clinical application of hiPS cells, e.g., in heart repair after myocardial infarction, would require at least 10^9 cells. This amount would correspond to 1000 vials assuming a cell density of 10^6 cells per ml, and a fill volume of one vial as 1 ml. The manufacturing of hiPS cells needs to shift from the lab-scale to large-scale production, with establishing standards on the way to design and operate the processes.

Various works are found in the literature that aim at attaining good manufacturability of cells for therapeutic purposes. Darkins and Mandenius [5] demonstrated computer-aided design of large-scale manufacturing of hiPS cells by investigating different process alternatives. Hourd and Williams [6] discussed the development and innovation in the production and commercialization of advanced cell therapies and precision medicines including hiPS cells. Pigeau et al. [7] tackled the scale-up issue in producing allogeneic pluripotent stem cells using batches of up to 2000 L in single-use format. For human embryonic stem (hES) cells, Yeo et al. [8] integrated a perfusion culture platform with mathematical modeling to enhance the bioprocess productivity and facilitate optimization. Levine et al. [9] presented an overview of chimeric antigen receptor T cell production from an initial working cell bank through cell expansion, aseptic processing, logistics, and finally, cell processing facilities. The research on cell manufacturability has been expanding by involving multidisciplinary approaches

* Corresponding author.
E-mail address: sugiyama@chemsys.t.u-tokyo.ac.jp (H. Suigyama).
Peer review under responsibility of the Japanese Society for Regenerative Medicine.

https://doi.org/10.1016/j.reth.2019.04.012

including cell science, biochemistry, biochemical engineering, and process systems engineering.

The present work deals with the filling of the hiPS cells. The role of the process is the filling of liquid containing cultivated and suspended hiPS cells into vials for preservation and/or transportation, which are highly relevant in commercial manufacturing. One important parameter in filling is the lot size. In good manufacturing practice (GMP), the quality standard for pharmaceuticals, the term "lot" is defined by the US Food and Drug Administration (FDA) [10] as: "*Lot or batch means one or more components or finished devices that consist of a single type, model, class, size, composition, or software version that are manufactured under essentially the same conditions and that are intended to have uniform characteristics and quality within specified limits.*" Kagihiro et al. [11] showed that the number of living cells decreases with the filling time, because the cells are damaged, e.g., by suspension, during filling. Thus, in determining the lot size, one has to pay attention to such a change in cell quality. For general cyclic production processes, Stefansdottir et al. [12] proposed classification schemes for setups and cleaning in lot sizing and scheduling for food production processes, and Groenevelt et al. [13] presented a log-sizing analysis considering machine breakdown. However, no contribution has dealt with lot sizing in the cell manufacturing processes, including the filling of hiPS cells.

Here, we present a distribution-based approach that can be used for determining lot sizes in the filling of hiPS cells. A key assumption was that a hiPS cell has "survival capability", which can be described by a lognormal distribution. The developed approach expresses the decrease in survival capability during filling, i.e., the change in cell quality, as "trimming" of the distribution. The distributions after different filling times are calculated, to be compared with the distribution of the initial filling time regarding the yield of the cells and the similarity. These comparison results are used as the quality constraints in determining the lot size. We present a mock-up case study of lot size optimization considering an economic objective as well as quality constraints. The novelty of the work is in the integrated nature of the model for lot size simulation and determination, which was built on top of the experimental findings by Kagihiro et al. [11].

2. Method

2.1. Process overview

An overview of the process investigated in the study is presented in Fig. 1. First, the liquid containing hiPS cells is suspended after cultivation by dissociation and centrifuge, and is retained in a vessel. The solution is then filled into vials, during which it is continuously suspended to maintain homogeneity. The filled vials are cryopreserved, and thawed at the point of use. Finally, the cells are attached for further processes such as cultivation or differentiation. The three steps of filling of the suspended cells, cryopreservation/thawing, and attachment are referred to as S, C, and A in the various subscripts of associated parameters. The retention vessel, the tubes, and the filling needles are assumed to be single-use materials, i.e., precleaned and sterilized, one-way use, and resin-made materials [14]. The filling is carried out by a peristaltic pump, and the system is assumed to be equipped with multiple filling needles to fill multiple vials simultaneously.

The lot size of the filling process, V_L [L], is defined as the initial volume of the liquid in the retention vessel. According to GMP, the content in one lot size needs to have a uniform quality; this well-established quality standard for pharmaceutical products was reflected in the determination of V_L. The relationship between V_L and the key process parameters is described in Eq. (1):

$$V_L = h \cdot u \cdot t_S \tag{1}$$

where u [L s^{-1}], h [−], and t_S [s] represent the filling rate, the number of filling needles, and the time spent filling, respectively. When appropriate, the unit of hour is used for t_S in this paper.

During the steps of filling, cryopreservation/thawing, and attachment, the hiPS cells are damaged, as shown by Kagihiro et al. [11]. They measured the ratio of the living and dead cells, i.e., the survival ratio, in each of the three steps at $t_S = \{0, 1, 2, 4\}$ h. It was observed that, in the steps of filling and attachment, the survival ratio decreased with the increasing t_S, whereas in cryopreservation/thawing, there was no strong relationship between the survival ratio and t_S. Overall, with increasing t_S, the number of live cells after the attachment step changed. Thus, in determining V_L, the change in the quality of the suspended cells needs to be considered.

2.2. Describing cell survival capability using probability distribution

To deal with the life and death of the cells quantitatively, we assumed that the survival capability of the hiPS cells could be described by a continuous probability distribution. It is natural to consider that the characteristics of biological objects follow a certain distribution, and this would be the case for hiPS cells. However, to date, little has been reported on such distribution information for hiPS cells. As an alternative, the following two characteristics were adopted in this work. The first is the dynamic viscoelasticity. In the field of microrheology, dynamic viscoelasticity and related phenomena have been measured for different biological objects such as erythrocytes [15], human airway smooth muscle cells [16], or the cell fluid of hES and hiPS cells [17]. Cai et al. [18] investigated the dynamic viscoelasticity of mouse fibroblast NIH3T3 cells, and presented the complex share modulus, G^* [Pa], using a complex number i in Eq. (2):

$$G^* = G_0 g(\alpha)\{1 + i\eta(\alpha)\}\left(\frac{f}{f_0}\right)^{\alpha} + i\mu f \tag{2}$$

where G_0 [Pa] is the scale factor of the modulus when the frequency factor f [Hz] is f_0 (= 1 Hz), α is a power-law exponent [−], and μ is the Newtonian viscous damping coefficient [Pa s]. The functions $g(\alpha)$ and $\eta(\alpha)$ represent $\Gamma(1-\alpha)\cos(\pi\alpha/2)$ and $\tan(\pi\alpha/2)$, respectively. Based on the measurement, Cai et al. [18] defined the parameters of α, G_0, and μ as normal distributions N (mean, standard deviation) as shown in Eqs. (3-1)–(3-3).

$$\alpha = N(0.32,\ 0.08) \tag{3-1}$$

$$\ln(G_0) = N(4.56,\ 0.62) \tag{3-2}$$

$$\ln(\mu) = N(-0.288,\ 0.65) \tag{3-3}$$

The second characteristic is the maximum elastic strain energy, E_{max} [J], the energy that a spherical solid object can accumulate until its collision. Kanda et al. [19] defined E_{max} as in Eq. (4):

$$E_{max} = 0.832\left(\frac{1-\nu^2}{Y}\right)^{\frac{2}{3}}\left(\frac{1}{2r}\right)^{\frac{1}{3}}F^{\frac{5}{3}} \tag{4}$$

where ν is the Poisson's ratio [−], Y is the Young's modulus [Pa], r is the radius of the sphere [m], and F is the load [N]. The expression of Y^*, Young's modulus using a complex number, as a function of G^* can be found, e.g., in Ref. [20], as shown in Eq. (5).

$$Y^* = 2(1+\nu)G^* \tag{5}$$

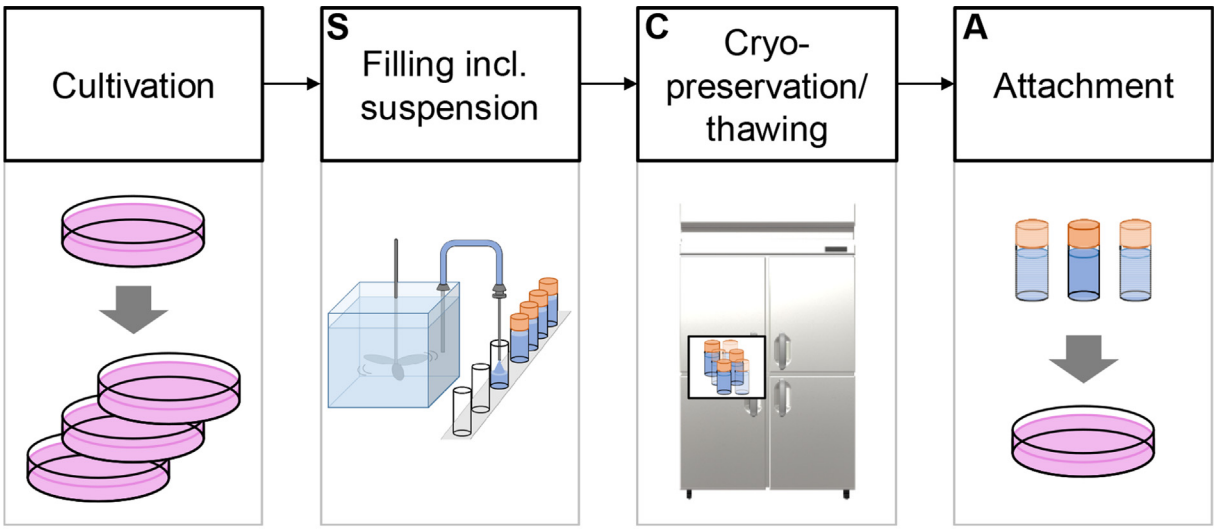

Fig. 1. Overview of the investigated process.

By replacing Y in Eq. (3) with $|Y^*|$ in Eq. (4), i.e., considering the maximum amount for Y, E_{max} can be rewritten as in Eq. (6):

$$\begin{aligned} E_{max} &= 0.832\left(\frac{1-\nu^2}{Y}\right)^{\frac{2}{3}}\left(\frac{1}{2r}\right)^{\frac{1}{3}}F^{\frac{5}{3}} \\ &= 0.832\left(\frac{1-\nu}{2}\right)^{\frac{2}{3}}\left(\frac{1}{2r}\right)^{\frac{1}{3}}F^{\frac{5}{3}} \times |G^*|^{-\frac{2}{3}} \\ &= q \times |G^*|^{-\frac{2}{3}} \end{aligned} \tag{6}$$

where q [$Pa^{2/3}$ J] is a coefficient that contains constant parameters before $|G^*|^{-\frac{2}{3}}$, which is defined for simplification. Because $|G^*|^{-\frac{2}{3}}$ follows a probability distribution determined by Eqs. (2) and (3), E_{max} has a distributed nature as well.

In this work, E_{max} (Eq. (6)) was defined as a pseudo indicator of the survival capability of a hiPS cell. Each cell follows the distribution of E_{max}, as does a group of cells in a retention vessel or in a filled vial. Because of the lack of distribution-related information on the hiPS cells, alternative characteristics, namely the dynamic viscoelasticity of mouse fibroblast NIH3T3 cells and the elastic strain energy of solid particles, had to be adopted. However, the indicator could still meet the purpose of the work, which was to demonstrate the effectiveness of the distribution-based approach for lot size determination rather than report calculated results.

For the distributed part of E_{max}, namely $|G^*|^{-\frac{2}{3}}$, a lognormal distribution, $f_\Lambda(x)$, described in Eq. (7) was found as the best fitting probability distribution:

$$f_\Lambda(x) = \frac{1}{\sqrt{2\pi}\nu x}\exp\left(-\frac{(\ln(x)-m)^2}{2\nu^2}\right) \tag{7}$$

where m and ν represent the parameters of $f_\Lambda(x)$, and x is the support of the function $(0, \infty)$. By comparing $f_\Lambda(x)$ with $|G^*|^{-\frac{2}{3}}$ using Monte Carlo simulation (#iteration = 10,000), the most likely values of m and ν were found to be −3.71 and 0.436, respectively. The distribution $f_\Lambda(x)$ represents the survival capability of the cells obtained in the cultivation, and is referred to as the initial distribution.

2.3. Judging life or death of cells using cell survival capability

In what follows, the algorithm for judging life or death of a cell is presented. Eqs. (8-1)–(8-3) describe the damage caused to a cell during filling, cryopreservation/thawing, and attachment, respectively:

$$E_S(t_S) = S_1 t_S + S_2 = q(s_1 t_S + s_2) \tag{8-1}$$

$$E_C(t_S) \geq 0 \tag{8-2}$$

$$E_A(t_S) = A_1 t_S + A_2 = q(a_1 t_S + a_2) \tag{8-3}$$

where S_1 [J s^{-1}] and A_1 [J s^{-1}], and S_2 [J] and A_2 [J] represent the proportionally constant and intercept regarding t_S, respectively. The parameters s_1 [$Pa^{-2/3}$ s^{-1}], s_2 [$Pa^{-2/3}$], a_1 [$Pa^{-2/3}$ s^{-1}], and a_2 [$Pa^{-2/3}$] correspond to S_1, S_2, A_1, and A_2, respectively, after the deformation to separate q. The dependency of the damage on t_S in each step was determined based on the characteristics reported by Kagihiro et al. [11]. The strategy in this work is to compare the types of damage defined in Eqs. (8-1)–(8-3) with the distribution of E_{max} to quantify the probability of cell survival at each step. For the actual calculation, $s_1 t_S + s_2$ and $a_1 t_S + a_2$ are compared with $f_\Lambda(x)$. Apart from the abovementioned types of damage, the cells regain the survival capability in the attachment step, which is the preparation status for growth. This aspect will be considered in a later part in this section. The parameters s and a describe the effect of suspension on the cell survival capability. The parameters s_1 and a_1 describe the t_S-proportional damage during the filling step; s_2 and a_2 are independent of t_S, and reflect the damage induced during the dissociating and centrifuge steps as the preparation for filling.

The effect of the damage during filling is described in Eqs. (9-1)–(9-3). Eq. (9-1) defines $f_{\Lambda_S}(x, t_S)$, the distribution of $f_\Lambda(x)$ after a filling time t_S, where the t_S-proportional damage to the cell is included. Eq. (9-2) defines the judgment criteria for the life and death of the cell using the distribution of f_{Λ_S}. Eq. (9-3) expresses the yield of the cells in the filling step, y_S [−], where an error function-based function $R(x')$, defined in Eq. (10), is used for the sake of simplification.

$$f_{\Lambda_S}(x, t_S) = f_\Lambda(x + (s_1 t_S + s_2)) \tag{9-1}$$

$$\begin{cases} x>0 & life \\ x\le 0 & death \end{cases} \tag{9-2}$$

$$y_S(t_S)=\frac{\int_0^\infty f_\Lambda(x+(s_1t_S+s_2))dx}{\int_0^\infty f_\Lambda(x+s_2)dx}=\frac{R(s_1t_S+s_2)}{R(s_2)} \tag{9-3}$$

$$R(x')=1-\frac{1}{2}erfc\left(-\frac{\ln(x')-m}{\sqrt{2}v}\right) \tag{10}$$

The second deformation in Eq. (9-3) was possible because f_Λ was expressed as a lognormal distribution. If other distributions were applied, an analytical expression of y_S could become difficult. In this case, Monte Carlo simulation can be used to obtain y_S numerically.

The effect of the damage during cryopreservation/thawing is described in Eqs. (11-1)–(11-4). Eq. (11-1) defines $f_{\Lambda_C}(x, t_S)$, the distribution of cell survival capability after both filling and cryopreservation/thawing steps, as a function of t_S. The t_S-independency during cryopreservation/thawing can be seen in the equation; the $f_{\Lambda_S}(x, t_S)$ distribution is "downsized" by the parameter c [−] defined in Eq. (11-2). Eqs. 11-3,11-4 express the probability of the life and death, and the yield of the cells in the cryopreservation/thawing step, respectively.

$$f_{\Lambda_C}(x,t_S)=c\times f_\Lambda(x+(s_1t_S+s_2)) \tag{11-1}$$

$$0\le c\le 1 \tag{11-2}$$

$$\begin{cases} p(life)=c \\ p(death)=1-c \end{cases} \tag{11-3}$$

$$y_C(t_S)=c \tag{11-4}$$

The effect of the damage during attachment is described in Eqs. (12-1)–(12-3). Eq. (12-1) defines $f_{\Lambda_A}(x, t_S)$ the cell survival capability distribution after all three steps as a function of t_S, where the t_S-proportional damage is expressed. As noted, the attachment step provides the environment where the cells could already grow, which is expressed by an "upsizing" parameter a_3 [−] (>1) in Eq. (12-1). Eq. (12-2) defines the judgment criteria for life and death using the initial distribution of f_{Λ_A}; Eq. (12-3) expresses the yield of the cells in the attachment step, y_A [−]. Similar to the case in Eq. (9-3), a Monte Carlo simulation can be applied to obtain y_A numerically, if the analytical expression is difficult.

$$f_{\Lambda_A}(x,t_S)=ca_3\times f_\Lambda(x+(s_1t_S+s_2)+(a_1t_S+a_2)) \tag{12-1}$$

$$\begin{cases} x>0 & life \\ x\le 0 & death \end{cases} \tag{12-2}$$

$$\begin{aligned} y_A(t_S)&=a_3\times\frac{\int_0^\infty f_\Lambda(x+(s_1t_S+s_2)+(a_1t_S+a_2))dx}{\int_0^\infty f_\Lambda(x+(s_1t_S+s_2))dx} \\ &=a_3\times\frac{R((s_1t_S+s_2)+(a_1t_S+a_2))}{R(s_1t_S+s_2)} \end{aligned} \tag{12-3}$$

The overall yield of the cells after the three steps, $y_{Overall}$ [−], is expressed as a function of t_S in Eq. (13).

$$y_{Overall}(t_S)=y_S(t_S)\cdot y_C(t_S)\cdot y_A(t_S) \tag{13}$$

The values of the parameters s_1, s_2, c, a_1, a_2, and a_3 can be calculated by comparing the stepwise yield with the experimental result, as presented by Kagihiro et al. [11]. In this work, the values of s_1 and s_2 were calculated by comparing $y_S|_{t_S=1}/y_S|_{t_S=0}$ and $y_S|_{t_S=2}/y_S|_{t_S=0}$ with the measured yield in the filling step at t_S = 1 h and 2 h (see Eq. (9-3)), respectively. The value of c (see Eq. (11-4)) was obtained directly from the measured yield in cryopreservation/thawing. The values of a_1 and a_2 were calculated by comparing $y_A|_{t_S=1}/y_A|_{t_S=0}$ and $y_A|_{t_S=2}/y_A|_{t_S=0}$ with the measured yield in the attachment step at t_S = 1 h and 2 h (see Eq. (12-3)), respectively. Finally, the parameter a_3 was specified by the increase in the number of cells that were obtained at t_S = 0 and were attached without cryopreservation/thawing. All values used were measured at room temperature in Ref. [11]. The values of s_1, s_2, c, a_1, a_2, and a_3 are included in Table 1.

2.4. Determining lot size using the overall yield and Cohen's d

The changes in the initial distribution, f_Λ, from cultivation through filling and cryopreservation/thawing, and finally to attachment are illustrated in Fig. 2. In the filling step, the weak cells with low E_{max} are eliminated; in cryopreservation/thawing, any cell has an equal possibility of being eliminated regardless of its E_{max}; in the attachment step, again, weak cells cannot survive. The distribution $f_{\Lambda_A}|_{x>0,t_S}$ represents the "consequential" survival capability of cells that are filled at the time point t_S, and immediately afterward are cryopreserved/thawed and attached. That means that by comparing $f_{\Lambda_A}|_{x>0,t_S}$ with $f_{\Lambda_A}|_{x>0,t_S=0}$, the cells filled at t_S and at t_S = 0 (the first vial) can be compared, which would lead to the determination of the lot size V_L (see Eq. (1)).

In this work, two indicators are used to compare two distributions, namely the overall yield, $y_{Overall}$ (see Eq. (13)), and Cohen's d [−] [21]. The indicator, $y_{Overall}$, quantifies the change in living cell density for the vial filled at t_S. With the increase in t_S, more cells would die, and cell density would decrease (Fig. 2). The density can be recovered, e.g., in the succeeding cultivation after the attachment step; however, a density discrepancy that is too large within a lot is undesirable. Thus, to consider the aspect of cell density in determining the lot size, a constraint could be set regarding $y_{Overall}$.

The other indicator, d, is a known effect size that is used to quantify the similarity of two distributions, $f_{\Lambda_A}|_{x>0,t_S}$ with $f_{\Lambda_A}|_{x>0,t_S=0}$. Eq. (14) shows the general definition of d using a stochastic variable X, mean of X, $\mu(X)$, standard deviation of X, $\sigma(X)$, and sample size n.

Table 1
Parameter values used in the calculation.

Symbol	Value	Unit	Remark
a_1	1.12×10^{-3}	[$Pa^{-2/3}\ s^{-1}$]	See Section 2.3.
a_2	4.93×10^{-3}	[$Pa^{-2/3}$]	See Section 2.3.
a_3	1.47	[−]	See Section 2.3.
c	8.25×10^{-1}	[−]	See Section 2.3.
C_{Change}	5.00×10^{4}	[JPY]	Set with reference to Ref. [23].
$C_{Tube/Needle}$	9.90×10^{4}	[JPY]	Set with reference to Ref. [23].
h	8	[−]	Assumed in this work.
m	− 3.71	[−]	See Section 2.2.
N_0	1.00×10^{2}	[L $year^{-1}$]	Assumed in this work.
s_1	4.1×10^{-3}	[$Pa^{-2/3}\ s^{-1}$]	See Section 2.3.
s_2	1.12×10^{-2}	[$Pa^{-2/3}$]	See Section 2.3.
u	1.00×10^{-4}	[L s^{-1}]	Assumed in this work.
v	4.36×10^{-1}	[−]	See Section 2.2.

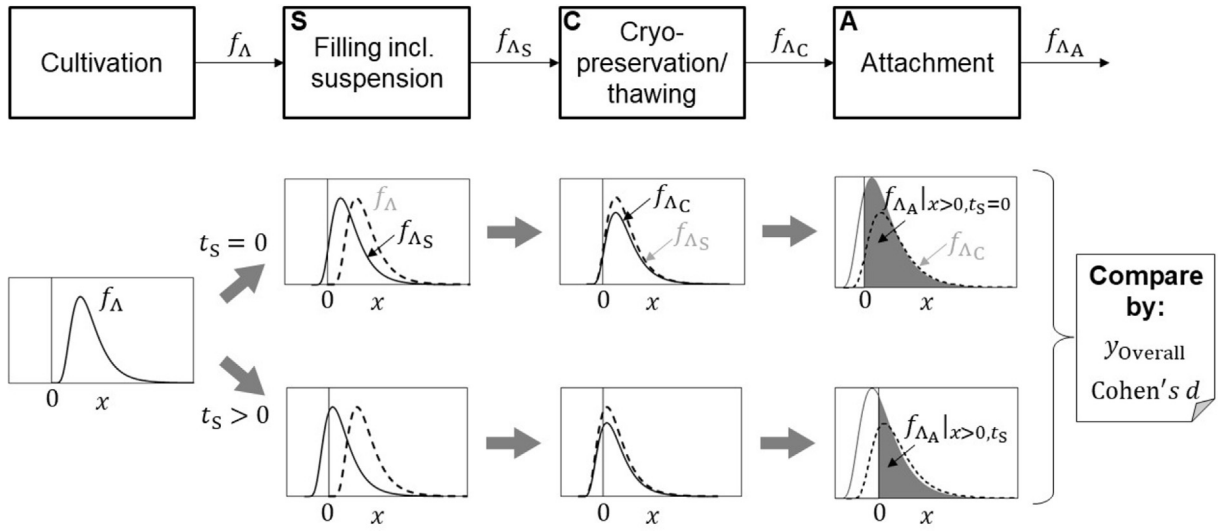

Fig. 2. Changes of the initial distribution, f_Λ, through the steps of filling, cryopreservation/thawing, and attachment.

$$d = \frac{|\mu(X_1) - \mu(X_2)|}{\sqrt{\frac{n_1\sigma(X_1)^2 + n_2\sigma(X_2)^2}{n_1+n_2}}} = \frac{\left|\mu\left(f_{\Lambda_A}|_{x>0,t_S}\right) - \mu\left(f_{\Lambda_A}|_{x>0,t_S=0}\right)\right|}{\sqrt{\frac{n_1\sigma\left(f_{\Lambda_A}|_{x>0,t_S}\right)^2 + n_2\sigma\left(f_{\Lambda_A}|_{x>0,t_S=0}\right)^2}{n_1+n_2}}} \quad (14)$$

Cohen's d becomes small when the two distributions are similar. As the standard, Cohen [22] defined three values of 0.2, 0.5, and 0.8, for a small, medium, and large effect, respectively. That means that when strict similarity is desired, as would be the case in hiPS cell filling, the value of 0.2 should be adopted. The second deformation in Eq. (14) is to present the adapted indicator d that investigates the difference between $f_{\Lambda_A}|_{x>0,t_S}$ and $f_{\Lambda_A}|_{x>0,t_S=0}$.

Because it is difficult to express the indicator d analytically, the value should be obtained numerically, e.g., by Monte Carlo simulation. In one run, random numbers can be sampled from $f_{\Lambda_A}|_{x,t_S}$ and $f_{\Lambda_A}|_{x,t_S=0}$, e.g., for 10,000, and then the data sets of $f_{\Lambda_A}|_{x>0,t_S}$ and $f_{\Lambda_A}|_{x>0,t_S=0}$ can be obtained by screening out negative values. These data sets can be used to calculate the indicator d. In the actual calculation of d, it was observed that the obtained d fluctuated in each run of the Monte Carlo simulation. This is seemingly caused by the skewed shape of the distribution of $f_{\Lambda_A}|_{x>0,t_S}$, which is influenced largely by the sampled values in the calculation. To improve reliability, it is suggested to repeat the set of Monte Carlo simulation multiple times, e.g., 10,000. After this double-loop calculation, the indicator d will be obtained as a probability distribution. Using the upper 5% point, $d^{0.05}$ [−], and the standard value of 0.2, we defined the judgment criteria on the similarity (Eq. (15)).

$$d^{0.05}(t_S) = 0.2 \quad (15)$$

Eqs. (13) and (15) constrain the possible time of t_S, i.e., the maximum value of the lot size V_L (see Eq. (1)). In Section 3, we introduce a case study in which the determination of V_L is presented by defining an economic objective function and quality constraints based on Eqs. (13) and (15).

3. Case study

3.1. Process description

The process shown in Fig. 1 was considered in a case study. It was assumed that the filling step had a retention bag with size V_L, a filling tube, and eight filling needles ($h = 8$, see Eq. (1)) that were connected sequentially. All materials were assumed to be single use. The annual demand of the cell, N_0, and the filling rate, u, were set as 100 L and 1.0×10^{-4} L s^{-1}, respectively. When the filling volume of a vial was 1 mL per vial, the rate u would correspond to 6 vial/min. The annual production cost, C_{Annual} [JPY year^{-1}], was defined in Eq. (16):

$$C_{Annual}(V_L) = \left(C_{Bag}(V_L) + C_{Tube/Needle} + C_{Change}\right)\frac{N_0}{V_L} \quad (16)$$

where C_{Bag} [JPY], $C_{Tube/Needle}$ [JPY], and C_{Change} [JPY] represent the costs of the retention bag, tube and filling needles, and lot changing over, respectively. These cost factors associated with single-use materials were set with reference to Shirahata et al. [23], who performed an economic evaluation of sterile filling processes using single-use materials. The factor C_{Bag} was formulated as a second-order function of V_L with an increasing tendency; otherwise, $C_{Tube/Needle}$ and C_{Change} were constant. The values used in the calculation are summarized in Table 1. The design problem was formulated as shown in Eq. (17).

$$\min_{V_L} C_{Annual}(V_L) \quad (17)$$

Subject to

$$V_L = h \cdot u \cdot t_S$$

$$y_{Overall}(t_S) \geq 0.8 \text{ or } 0.6 \text{ or } 0.4$$

$$d^{0.05}(t_S) \leq 0.2$$

$$0 \leq t_S \leq 3\text{h}$$

Here, C_{Annual} in Eq. (16) is defined as the objective function, or the indicator that should be minimized, in this case by varying V_L. The minimization is subject to the constraints. First, the relation

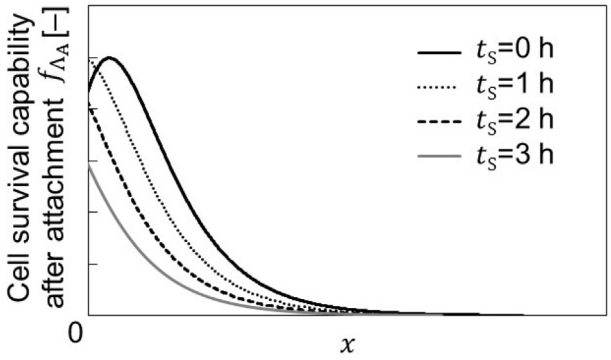

Fig. 3. Time change of the distribution of the consequential survival capability, $f_{\Lambda_A}|_{x>0,t_S}$.

between t_S and V_L is maintained as defined in Eq. (1). Second, $y_{Overall}$ in Eq. (13) should be above a certain target, which was set as 0.8, 0.6, or 0.4 in this study. Third, $d^{0.05}$ should be below the standard of 0.2, which was introduced in Eq. (15) as the criteria of similarity. Lastly, the range of t_S was set between 0 and 3 h. The second and third constraints represent the quality conditions that are uniquely defined in the lot sizing of hiPS cell filling.

3.2. Change in survival capability over filling time

The time change of the distribution $f_{\Lambda_A}|_{x>0,t_S}$ from $t_S = 0$ to 3 h is shown in Fig. 3 with 0.5 h increments. The shape of the distribution is skewed as illustrated in Fig. 2; as t_S increases, the trimmed area becomes larger, and the difference between $f_{\Lambda_A}|_{x>0,t_S}$ and $f_{\Lambda_A}|_{x>0,t_S=0}$ increases as well. This dynamic change will be assessed by the indices of $y_{Overall}$ regarding the area of the distribution, and $d^{0.05}$ regarding the shape of the distribution.

The time change of $y_{Overall}$, from 0 to 3 h is shown in Fig. 4 with 0.1 h increments. The values were obtained analytically using Eq. (13). Consistent with the result shown in Fig. 3, $y_{Overall}$ decreases with increasing t_S. Among the calculated t_S, the largest values that satisfied the second constraint in Eq. (17) were 8.06×10^{-1}, 1.61, and 2.58 h, for 0.8, 0.6, and 0.4 as $y_{Overall}$, respectively. The corresponding lot sizes V_L for these t_S were 2.32, 4.63, and 7.42 L, respectively.

The time change of Cohen's d is shown in Fig. 5. Unlike $y_{Overall}$, the indicator d was calculated numerically: at each t_S, a double-loop Monte Carlo simulation was performed, i.e., 10,000 samplings for $f_{\Lambda_A}|_{x,t_S}$ and $f_{\Lambda_A}|_{x,t_S=0}$, and this was repeated 10,000 times. With the increase in t_S, the distribution of d shifted upward. Among the

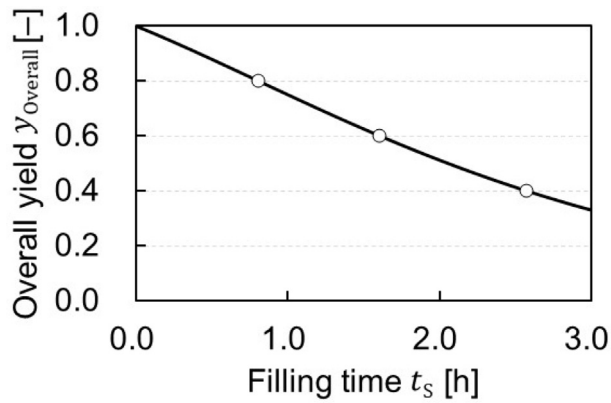

Fig. 4. Time change of the overall yield, $y_{Overall}$.

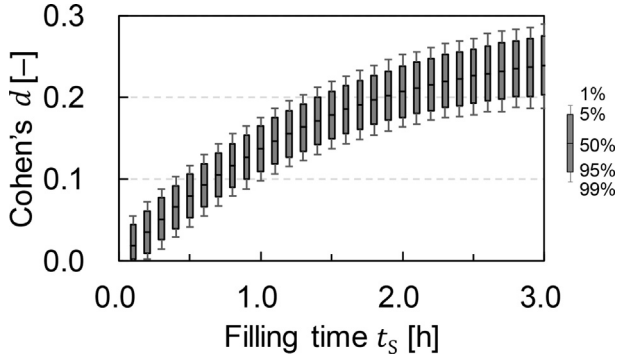

Fig. 5. Time change of Cohen's d.

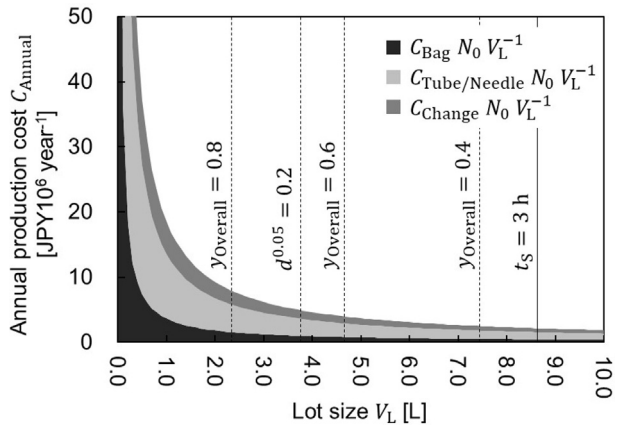

Fig. 6. Evaluation result of the annual operating cost, C_{Annual}, as a function of V_L indicating the constraints on overall yield, $y_{Overall}$, and Cohen's d.

calculated t_S, the largest value that satisfied the third constraint in Eq. (17) was 1.3 h, which corresponded to a V_L of 3.74 L.

3.3. Evaluation of cell survival capability and determination of the lot size

The evaluation result of the annual operating cost, C_{Annual}, is presented in Fig. 6 as a function of V_L, indicating the constraints on $y_{Overall}$ and Cohen's d using dotted lines. The corresponding value of V_L for $t_S = 3$ h, the upper bound of t_S indicated by a solid line, is 8.64 L. With the increase in V_L, the cost C_{Annual} decreases. Although C_{Bag} was defined as an increasing function of V_L, which could have affected the cost negatively, the effect was almost negligible. Values of $y_{Overall}$ and Cohen's d in the inequality constraints Eq. (17) are also presented in Fig. 6. Because C_{Annual} decreases monotonously, the inequality constraints determine the optimal solution of V_L. If the constraint $y_{Overall} \geq 0.8$ is adopted, then the constraint on $y_{Overall}$ already determines the optimal V_L as 2.32 L. If $y_{Overall} \geq 0.6$ or 0.4, the constraint on $d^{0.05}$ serves as a harder constraint, and the optimal V_L is given as 3.74 L. The corresponding $y_{Overall}$ at $V_L = 3.74$ L was 0.674. In this way, the constraints of $y_{Overall}$ and d compete in the determination of the optimal lot size.

4. Discussion

The obtained optimal V_L values were strongly affected by either of the two constraints on cell quality, which were expressed by $y_{Overall}$ and Cohen's d. In injectable manufacturing, where the quality degradation during filling may be less problematic than in

the cell manufacturing, the inequality constraints in Eq. (17) would not be necessary. In this case, the optimal lot size would be as high as the upper bound, and would be larger than the obtained V_L presented above. This difference could be interpreted as the difficulty of cell manufacturing, where the product quality could rapidly change during processing. Our integrated model presented this fundamental difference between cell and injectable filling quantitatively for the first time. Here, Cohen's d played an essential role in comparing the similarity of the filled cells from the initial state.

The result of C_{Total} decreased monotonously because the function mainly considered the single-use material costs associated with the production. However, in reality, the increase in filling time could increase the possibility of unexpected problems, e.g., machine failure, which could lead to the rejection of the entire lot in the worst case. Incorporation of such stochastic events in the evaluation, which was out of the scope here, could cause increase of C_{Total} after a certain filling time, leading to a different optimization result.

The approach can deal flexibly with different types of probability distribution specified for f_Λ. In the present case, where a lognormal distribution was used, an analytical expression of $y_{Overall}$ was possible, as presented in Eqs. 9-3,12-3. For other types, such as beta or Weibull distributions, the Monte Carlo simulation could be applied to quantify $y_{Overall}$, as was done for d. The remaining logic could stay the same for determining the appropriate lot size.

The specification of the initial distribution f_Λ would require more in-depth understanding of the cell actions. In the present study, the dynamic viscoelasticity of a different cell was adopted to describe the cell survival capability for the sake of demonstration. For hiPS cells, there could be a more appropriate and measurable characteristic that could be obtained as a probability distribution, e.g., degree of progress in cell apoptosis. In some conditions, hiPS cells are handled as aggregates, where the survival capability could be described differently from the case of single cells. The entire model still awaits for future validation with experimental data for evaluation, but again, the approach to determining the lot size could remain the same. This ready-to-be-run approach with the integrated mathematical models is the final output of the work.

5. Conclusions and outlook

In this work, we presented a distribution-based and conceptual approach for determining the lot size in the filling process of hiPS cells. The survival capability of the hiPS cells was assumed as a lognormal distribution, by referring to the dynamic viscoelasticity of mouse fibroblast NIH3T3 cells, and the elastic strain energy of solid particles. The decrease in capability was modeled based on reported experimental results for filling, cryopreservation/thawing, and attachment steps for hiPS cells. The distribution of the consequential survival capability of the cells filled at different time points was formulated as a function of filling time. By analyzing the distribution using the overall yield and Cohen's d, the adequate filling time could be identified, which could be applied in determining the lot size.

To demonstrate the approach, a mock-up case study was performed. The design problem was formulated to minimize the annual production cost by varying the lot size, subject to the constraints on cell yield and given the constraints of the difference in survival capability. The result indicated that the objective function decreased monotonously, and the highest lot size was determined as the optimal lot size. Because the input information was based on a different type of cells, the reported results cannot be used directly in practice. However, the approach would remain the same when actual distribution information on hiPS cells becomes quantified and available.

The following points can be explored as future research opportunities. First, the determination of the cell survival capability could be addressed by considering various biological activities to run the approach and obtain meaningful results. Second, the elaboration of the objective function would be desired. Incorporation of the undesired but possible failure events could penalize a long filling time, which could lead to the estimation of a more useful lot size. Lastly, systems engineering approaches as presented in this work could be extended to cover other processes for the industrial manufacturing of hiPS cells. To achieve good cell manufacturability for hiPS cells, establishment of a systems fundament for the entire process would be necessary.

Declarations of interest

None.

Acknowledgments

The authors acknowledge the useful discussions with Drs. Ikki Horiguchi and Kazuhiro Fukumori from Osaka University, and Prof. Masahiko Hirao from The University of Tokyo. We thank Mr. Yusuke Hayashi from The University of Tokyo for assistance in the literature review. This study was supported by the Japan Agency for Medical Research and Development (AMED) in the project “Development of cell manufacturing and processing system for industrialization of regenerative medicine” (No. P14006). H.S. appreciates the financial support from a Grant-in-Aid for Young Scientists (B) No. 26820343 and (A) No. 17H04964 from the Japan Society for the Promotion of Science (JSPS) as well as Research Grant 2017 from the Nagai Foundation Tokyo.

Nomenclature

A_1	Coefficient associated with attachment [J s^{-1}]
a_1	Coefficient associated with attachment [$Pa^{-2/3}$ s^{-1}]
A_2	Coefficient associated with attachment [J]
a_2	Coefficient associated with attachment [$Pa^{-2/3}$]
a_3	Coefficient associated with attachment [−]
c	Coefficient associated with cryopreservation [−]
C_{Annual}	Annual production cost [JPY $year^{-1}$]
C_{Bag}	Cost of retention bag per lot [JPY]
C_{Change}	Cost of changing lot [JPY]
$C_{Tube/Needle}$	Cost of tubes and needles per lot [JPY]
E_{Max}	Maximum elastic strain energy of a cell [J]
E	Damage to a cell [J]
F	Load [N]
f	Frequency factor [Hz]
f_0	Unit frequency factor (1 Hz)
f_Λ	Lognormal distribution of cell survival capability after cultivation, i.e., initial distribution
f_{Λ_S}	Distribution of cell survival capability after filling
f_{Λ_C}	Distribution of cell survival capability after cryopreservation/thawing
f_{Λ_A}	Distribution of cell survival capability after attachment
G_0	Scale factor of the modulus at f_0 [Pa]
G^*	Complex share modulus [Pa]
h	Number of filling needles [−]
i	Complex number
m	Parameter of lognormal distribution
n	Sample size [−]
N	Normal distribution
N_0	Annual production volume [L $year^{-1}$]
q	Constant [$Pa^{2/3}$ J]
$R(x')$	Function defined in Eq. (10)

r	Radius of a sphere [m]
S_1	Coefficient associated with filling [J s^{-1}]
s_1	Coefficient associated with filling [$Pa^{-2/3}$ s^{-1}]
S_2	Coefficient associated with filling [J]
s_2	Coefficient associated with filling [$Pa^{-2/3}$]
t_S	Time for filling [s]
u	Filling rate [L s^{-1}]
ν	Parameter of lognormal distribution
V_L	Lot size [L]
x	Support of the function
X	Stochastic variable
Y	Young's modulus [Pa]
y_S	Yield in filling [−]
y_C	Yield in cryopreservation/thawing [−]
y_A	Yield in attachment [−]
$y_{Overall}$	Overall yield [−]
α	Power-law exponent [−]
$g(\alpha)$	Function of $\Gamma(1-\alpha)\cos(\pi\alpha/2)$
$\eta(\alpha)$	Function of $\tan(\pi\alpha/2)$
μ	Newtonian viscous damping coefficient [Pa s]
$\mu(X)$	Mean of stochastic variable X
$\sigma(X)$	Standard deviation of stochastic variable X
ν	Poisson's ratio [−]

References

[1] Kamao H, Mandai M, Okamoto S, Sakai N, Suga A, Sugita S, et al. Characterization of human induced pluripotent stem cell-derived retinal pigment epithelium cell sheets aiming for clinical application. Stem Cell Rep 2014;2:205–18.

[2] Kawamura M, Miyagawa S, Miki K, Saito A, Fukushima S, Higuchi T, et al. Feasibility, safety, and therapeutic efficacy of human induced pluripotent stem cell-derived cardiomyocyte sheets in a porcine ischemic cardiomyopathy model. Circulation 2012;126:S29–37.

[3] Takebe T, Sekine K, Kimura M, Yoshizawa E, Ayano S, Koido M, et al. Massive and reproducible production of liver buds entirely from human pluripotent stem cells. Cell Rep 2017;21:2661–70.

[4] Olmer R, Haase A, Merkert S, Cui W, Paleček J, Ran C, et al. Long-term expansion of undifferentiated human iPS and ES cells in suspension culture using a defined medium. Stem Cell Res 2010;5:51–64.

[5] Darkins CL, Mandenius CF. Design of large-scale manufacturing of induced pluripotent stem cell derived cardiomyocytes. Chem Eng Res Des 2014;92:1142–52.

[6] Hourd P, Williams DJ. Scanning the horizon for high value-added manufacturing science: accelerating manufacturing readiness for the next generation of disruptive, high-value curative cell therapeutics. Cytotherapy 2018;20:759–67.

[7] Pigeau GM, Csaszar E, Dulgar-Tulloch A. Commercial scale manufacturing of allogeneic cell therapy. Front Med 2018;5:1–8.

[8] Yeo D, Kiparissides A, Cha JM, Aguilar-Gallardo C, Polak JM, Tsiridis E, et al. Improving embryonic stem cell expansion through the combination of perfusion and bioprocess model design. PLoS One 2013;8:e81728.

[9] Levine BL, Miskin J, Wonnacott K, Keir C. Global manufacturing of CAR T cell therapy. Mol Ther – Methods Clin Dev 2017;4:92–101.

[10] US Food and Drug Administration (US FDA). Title 21: food and drugs, Part 820—quality system regulation, subpart A—general provisions, §820.3 definitions. Available online at: http://www.ecfr.gov/cgi-bin/text-idx?SID=42e63945e733bc1064816ff14a509b72&mc=true&node=pt21.4.211&rgn=div5. [Accessed 23 October 2018].

[11] Kagihiro M, Fukumori K, Aoki T, Ungkulpasvich U, Mizutani M, Viravaidya-Pasuwat K, et al. Kinetic analysis of cell decay during the filling process: application to lot size determination in manufacturing systems for human induced pluripotent and mesenchymal stem cells. Biochem Eng J 2018;131:31–8.

[12] Stefansdottir B, Grunow M, Akkerman R. Classifying and modeling setups and cleanings in lot sizing and scheduling. Eur J Oper Res 2017;261:849–65.

[13] Groenevelt H, Pintelon L, Seidmann A. Production lot sizing with machine breakdowns. Manag Sci 1992;38:104–23.

[14] Eibl R, Eibl D, editors. Single-use technology in biopharmaceutical manufacture. Hoboken, NJ: John Wiley & Sons, Inc.; 2011.

[15] Fischer TM, Stohr-Liesen M, Schmid-Schonbein H. The red cell as a fluid droplet : tank tread-like motion of the human erythrocyte membrane in shear flow. Science 1978;202:894–6.

[16] Fabry B, Maksym GN, Butler JP, Glogauer M, Navajas D, Fredberg JJ. Scaling the microrheology of living cells. Phys Rev Lett 2001;87:1–4.

[17] Daniels BR, Hale CM, Khatau SB, Kusuma S, Dobrowsky TM, Gerecht S, et al. Differences in the microrheology of human embryonic stem cells and human induced pluripotent stem cells. Biophys J 2010;99:3563–70.

[18] Cai P, Mizutani Y, Tsuchiya M, Maloney JM, Fabry B, Van Vliet KJ, et al. Quantifying cell-to-cell variation in power-law rheology. Biophys J 2013;105:1093–102.

[19] Kanda Y, Toshihiro K, Yasuo K, Torajiro H, Saburou Y. Possibility of micronizing using ball mill pulverization. J Min Metall Inst Jpn 1985;102:581–4.

[20] Meyers MA, Chawla KK. Mechanical behavior of materials. 2nd ed. Cambridge, New York: Cambridge University Press; 2009.

[21] Cohen J. Statistical power analysis for the behavioral sciences. 2nd ed. Hillsdale, New Jersey: L. Erlbaum Associates; 1988.

[22] Cohen J. A power primer. Psychol Bull 1992;112:155–9.

[23] Shirahata H, Hirao M, Sugiyama H. Decision-support method for the choice between single-use and multi-use technologies in sterile drug product manufacturing. J Pharm Innov 2017;12:1–13.